universe

MDPI

Article

Analog Particle Production Model for General Classes of Taub-NUT Black Holes

Joshua Foo [1,*], Michael R. R. Good [2] and Robert B. Mann [3,4]

[1] Centre for Quantum Computation & Communication Technology, School of Mathematics & Physics, University of Queensland, St. Lucia, QLD 4072, Australia
[2] Energetic Cosmos Laboratory, Physics Department, Nazarbayev University, Nur-Sultan 010000, Kazakhstan; michael.good@nu.edu.kz
[3] Department of Physics & Astronomy, University of Waterloo, Waterloo, ON N2L 3G1, Canada; rbmann@uwaterloo.ca
[4] Institute for Quantum Computing, University of Waterloo, Waterloo, ON N2L 3G1, Canada
* Correspondence: joshua.foo@uqconnect.edu.au

Abstract: We derive a correspondence between the Hawking radiation spectra emitted from general classes of Taub-NUT black holes with that induced by the relativistic motion of an accelerated Dirichlet boundary condition (i.e., a perfectly reflecting mirror) in (1+1)-dimensional flat spacetime. We demonstrate that the particle and energy spectra is thermal at late times and that particle production is suppressed by the NUT parameter. We also compute the radiation spectrum in the rotating, electrically charged (Kerr–Newman) Taub-NUT scenario, and the extremal case, showing, explicitly, how these parameters affect the outgoing particle and energy fluxes.

Keywords: moving mirrors; QFT in curved spacetime; Hawking radiation

Citation: Foo, J.; Good, M.R.R.; Mann, R.B. Analog Particle Production Model for General Classes of Taub-NUT Black Holes. *Universe* **2021**, *7*, 350. https://doi.org/10.3390/universe7090350

Academic Editor: Stefano Bellucci

Received: 24 August 2021
Accepted: 17 September 2021
Published: 20 September 2021

1. Introduction

Taub-NUT black holes are a simple yet instructive electrovacuum solution to the Einstein–Maxwell field equations [1,2]. The Taub-NUT metric is a generalisation of the Schwarzschild metric with the addition of the so-called NUT parameter, l, and has played an important role in our understanding of the AdS/CFT correspondence [3–6]. Its initial discovery by Taub [1] and the subsequent coordinate extension applied to it by Newman, Unti and Tamburino (NUT) [2], led to the eventual discovery of the well-known rotating Kerr black hole solution [7].

In this paper, we propose a simple, (1+1)-dimensional model describing the Hawking radiation [8] properties of general classes of Lorentzian Taub-NUT black holes, known as the accelerated boundary correspondence (ABC). The model associates the origin of the black hole coordinates in (3+1)-dimensions with the trajectory of an accelerated mirror (i.e., a perfectly reflecting boundary) in (1+1)-dimensional Minkowski spacetime [9–11]. The relativistic trajectory of the mirror, which rapidly changes the boundary conditions of incoming field modes, induces particle production from the quantum vacuum [12,13]. Recently, this model has been applied to the well-known Schwarzschild [14], Reissner–Nordström (RN) [15], Kerr [16] and Kerr–Newman metrics [17], where analytic expressions for the spectra and the late-time thermal emission were derived.

We extend upon the aforementioned studies by considering general classes of Taub-NUT black holes, including those with a non-zero angular momentum and charge. Motivated by prior insights gleaned regarding the effect of spin and charge on the radiation, here, we ask how the presence of the NUT charge affects particle production and energy emission. Our results show that, in general, the presence of the NUT charge inhibits particle production for non-extremal black holes. Meanwhile, for the extremal (rotating, electrically and NUT charged) case, we find that the particle and energy spectrum is non-monotonic

with an increasing l. The utility of the ABC approach lies in its ability to elicit simple, closed-form expressions for the aforementioned quantities without relying on approximations which have been known to breakdown in certain regimes [18].

Our paper is organised as follows: In Section 2, we introduce the field-theoretic details for the Taub-NUT metric and the associated mirror trajectory in (1+1)-dimensional Minkowski spacetime. We, then, calculate the energy and particle spectrum of the outgoing radiation, demonstrating its thermal character at late times. In Section 3, we extend our analysis to the rotating, electrically charged version of the Taub-NUT spacetime (Kerr–Newman Taub-NUT, or KNTN). We conclude with some final remarks in Section 5. In the Appendices A–C, we derive a new class of mirror trajectories associated with a Taub-NUT spacetime with a vanishing two-space curvature, $\varepsilon = 0$, where we discover a thermal spectrum at *early times*. We conjecture that the mirror trajectory and ensuing particle creation reflects black hole dynamics with a reversal of time, since in the $\varepsilon = 0$ case, time becomes a space-like coordinate and vice versa. Throughout this paper, we utilise natural units, $G = c = \hbar = k_B = 1$.

2. Accelerated Boundary Correspondence

2.1. Taub-NUT Metric

The Taub-NUT metric is often expressed in the form:

$$\mathrm{d}s^2 = -f(r)\left(\mathrm{d}\bar{t} - 2l\cos\theta\mathrm{d}\phi\right)^2 + \frac{\mathrm{d}r^2}{f(r)} + (r^2 + l^2)\mathrm{d}\Theta^2, \tag{1}$$

where $\mathrm{d}\Theta^2 = \mathrm{d}\theta^2 + \sin^2\theta\mathrm{d}\phi^2$ and:

$$f(r) = \frac{r^2 - 2Mr - l^2}{r^2 + l^2}. \tag{2}$$

In the limit $l \to 0$, the metric reduces to the well-known Schwarzschild solution and M takes on the interpretation of the mass of the source. The metric Equation (1) has two Killing horizons but no curvature singularity. The physical meaning of the NUT parameter, l, remains an open question; it is commonly interpreted as a magnetic mass parameter [18]; however, other investigations have associated it with the twisting parameter of the source-free electromagnetic field within which a Schwarzschild black hole resides [19]. The parameter l relaxes global asymptotic flatness (e.g., singularity at $\theta = \pi$) despite the Riemann tensor scaling at r^{-3} at infinity [20].

Associated with the NUT charge l is a singularity on the polar axis known as a Misner string (an analogue of the Dirac string singularity in electromagnetism) and regions of spacetime in its vicinity having closed time-like curves. Traditionally, these issues have been avoided by imposing the periodicity of the time coordinate [21], rendering the string unobservable. This, consequently, leads not only to the existence of closed time-like curves everywhere, but additionally makes the maximal extension of the spacetime problematic [21,22]. However, it has recently been shown that the spacetime described by the metric Equation (1) is geodesically complete and free from causal pathologies for freely falling observers if time periodicity is not imposed [23,24]. Indeed, the Misner string is transparent to geodesics, and the spacetime has no closed time-like or null geodesics, provided some restrictions are imposed on the parameters of the NUT solution. Furthermore, the Kruskal extension through both horizons can be carried out if there is no time periodicity [25], and it is possible to formulate a consistent thermodynamics of Taub-NUT spacetime with Misner strings present [26–29].

Because of the string singularity at $\theta = \pi$, one can perform the transformation $\bar{t} = t + 2l\phi$ to obtain the modified line element [20],

$$\mathrm{d}s^2 = -f(r)\left(\mathrm{d}t + 4l\sin^2\frac{\theta}{2}\mathrm{d}\phi\right)^2 + \frac{\mathrm{d}r^2}{f(r)} + (r^2 + l^2)\mathrm{d}\Theta^2. \tag{3}$$

There are two horizons, occurring at $r_\pm = M \pm \sqrt{M^2 + l^2}$, which define the so-called NUT regions, NUT$_-$ and NUT$_+$. Consider the simplified (1+1)-dimensional metric in a plane of $\theta = \phi =$ const., yielding the simplified metric,

$$\mathrm{d}s^2 = -f(r)\mathrm{d}t^2 + \frac{\mathrm{d}r^2}{f(r)}. \tag{4}$$

The thermal radiation emitted from the Taub-NUT black hole and detected by an inertial observer at infinity has the temperature:

$$T_{\mathrm{TN}} = \frac{\kappa_+}{2\pi}, \tag{5}$$

where

$$\kappa_+ = \frac{1}{2}\frac{\mathrm{d}f(r)}{\mathrm{d}r}\bigg|_{r=r_+} = \frac{1}{2}\left(M + \sqrt{M^2 + l^2}\right)^{-1}, \tag{6}$$

is the usual surface gravity at the outer horizon. From Equation (5), we saw, explicitly, that the temperature of the black hole decreases with increasing l. This is reminiscent of the cooling effect that both charge and angular momentum have on the temperature of the RN and Kerr black holes, respectively. We introduced a tortoise coordinate, obtained via:

$$r^\star = \int \frac{\mathrm{d}r}{f(r)}, \tag{7}$$

which yields:

$$r^\star = r + \sqrt{M^2 + l^2}\ln\left|\frac{r - r_+}{r - r_-}\right| + M\ln\left|\frac{(r - r_+)(r - r_-)}{r_S^2}\right|, \tag{8}$$

where $r_S \equiv 2M$ is the usual Schwarzschild radius, and an integration constant is chosen so that our results coincide with the Schwarzschild limit derived in [14], as $l \to 0$.

2.2. Taub-NUT Mirror

The tortoise coordinate Equation (8) can be used to define a double null coordinate system, (u, v), where $u = t - r^\star$ and $v = t + r^\star$, for the exterior geometry of the black hole, which allows the line element to be written in the form:

$$\mathrm{d}s^2 = -f\,\mathrm{d}u\mathrm{d}v. \tag{9}$$

One then employs a matching condition (see [13]) with the flat interior geometry, which is described by the interior coordinates:

$$U = T - r, \qquad V = T + r, \tag{10}$$

and associates this condition with the mirror trajectory, corresponding to the $r = 0$ coordinate. The matching condition expresses the exterior function, $u(U)$, in terms of the interior coordinate U. To perform this, we set $r = r^\star$, and took $r^\star(r = (v_0 - U)/2) = (v_0 - u)/2$ along a light ray, v_0. Using this condition, we obtained two possible conditions for v_0, namely, $v_0 - 2r_\pm = v_H$ where v_H is the null coordinate of the horizon. Anticipating a transition to the (1+1)-dimensional mirror system, we could neglect the inner horizon solution, which occurs at $r < 0$; the trajectory of the mirror (i.e., the reflecting point for incoming field modes) models the $r = 0$ coordinate in the black hole coordinate system. More specifically, the particular choice of the light ray $v_0 - 2r_\pm = v_H$ gave us the analog to the outer horizon of the black hole. Since the field modes are lost to the left after $t = -x$ (the acceleration horizon of the mirror, see Figures 1 and 2), the inner horizon has a negligible role to play in determining the spectrum as seen by an observer on the right.

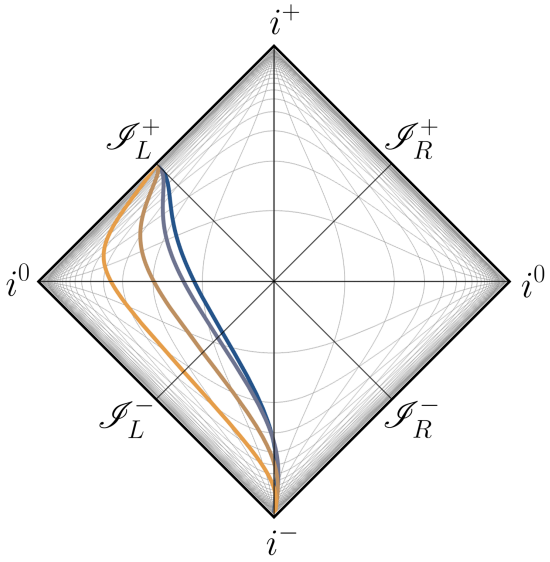

Figure 1. Penrose conformal diagram of the analog Taub-NUT mirror trajectories, with $l = 0.5$ and $M = 0.125, 0.25, 0.5, 1$, ranging from dark blue to orange. Recall that we utilised natural units, setting $G = c = \hbar = k_B = 1$.

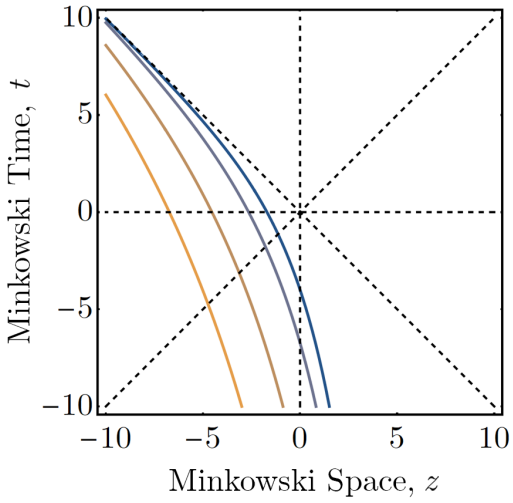

Figure 2. Spacetime diagram of the trajectories shown in Figure 1. These trajectories highlight the late-time acceleration horizon that mimics the formation of the black hole event horizon.

Applying these conditions to the tortoise coordinate, we obtained the exterior coordinate, $u(U)$, given by:

$$u(U) = U - \frac{1}{\kappa_+} \ln \left| \frac{U}{4M} \right| - \frac{1}{\kappa_-} \ln \left| \frac{U - 4\sqrt{M^2 + l^2}}{4M} \right|, \tag{11}$$

where

$$\frac{1}{\kappa_\pm} = 2M \pm 2\sqrt{M^2 + l^2}, \tag{12}$$

are the inverse surface gravities of the outer and inner horizons, respectively.

As already mentioned, the accelerated boundary correspondence associates the origin of the black hole geometry with the trajectory of a perfectly reflecting point in (1+1)-dimensional Minkowski spacetime (i.e., our accelerated Dirichlet boundary condition).

Making the identification $f(v) \Leftrightarrow u(U)$ (where $f(v)$ is commonly known as the ray-tracing function [12], i.e., it is the EoM trajectory of the mirror), we obtained:

$$f(v) = v - \frac{1}{\kappa_+} \ln|\kappa_S v| - \frac{1}{\kappa_-} \ln|\kappa_S(v - 4\psi)|, \tag{13}$$

where $\kappa_S = 1/4M$ is the surface gravity of the Schwarzschild black hole and we defined $\psi = \sqrt{M^2 + l^2}$. These black hole parameters retain their usual interpretation in the (1+1)-dimensional system, and their effect is to modify the spacetime trajectory of the mirror. It is straightforward to verify that this reduces to the Schwarzschild mirror trajectory in the limit $l \to 0$ [14]. The rapidity $\eta(v)$ as a function of advanced time is given by $-2\eta(v) = \ln f'(v)$. For the Taub-NUT analog mirror, we obtained:

$$\eta(v) = -\frac{1}{2} \ln\left|1 - \frac{1}{\kappa_+ v} + \frac{1}{4\kappa_-(\psi - v)}\right|, \tag{14}$$

which approaches the speed of light near the horizon, $v \to 0^-$. To the leading order in v, the late-time proper acceleration, $\alpha(v) = e^{\eta(v)}\eta'(v)$, is given by:

$$\lim_{v \to 0^-} \alpha(v) = -\frac{\kappa_+}{\sqrt{-4\kappa_+ v}}. \tag{15}$$

which is divergent. At early times, $v \to -\infty$, the mirror is static, as can be seen in the conformal Penrose diagram of Figure 1.

2.3. Energy Flux and Particle Spectrum

Having analysed the (1+1)-dimensional trajectory of the Taub-NUT analog mirror, we now considered the properties of outgoing particle and energy fluxes induced by its motion. The radiated energy flux, $F(v)$, can be calculated from the quantum stress-energy tensor using the simple expression [30],

$$F(v) = \frac{1}{24\pi}\{f(v), v\} f'(v)^{-2}, \tag{16}$$

where the Schwarzian brackets are defined as:

$$\{f(v), v\} = \frac{f'''}{f'} - \frac{3}{2}\left(\frac{f''}{f'}\right)^2. \tag{17}$$

To the leading order in v, near $v \to 0^-$, we discovered a constant energy flux:

$$F(v) = \frac{\kappa_+^2}{48\pi} + \mathcal{O}(v^2). \tag{18}$$

This behaviour is comparable to the analog mirror trajectories for the Kerr and Kerr–Newman black holes [16,17], and is indicative of late-time thermal behaviour.

Next, we considered the particle spectrum of the outgoing modes. This can be derived from the Bogoliubov coefficients,

$$\beta_{\omega\omega'} = \frac{1}{2\pi}\sqrt{\frac{\omega'}{\omega}} \int_{-\infty}^{v_H} \mathrm{d}v\, e^{-i\omega' v - i\omega f(v)}, \tag{19}$$

where ω, ω' are the frequencies of the outgoing and incoming modes, respectively. This is a simplified form of the inner product integral in, e.g., [30] where integration by parts neglects non-contributing surface terms. The particle spectrum can be obtained by taking the modulus square, $N^{\mathrm{TN}}_{\omega\omega'} := |\beta_{\omega\omega'}|^2$ which yields:

$$N^{\mathrm{TN}}_{\omega\omega'} = \frac{\omega'}{2\pi\kappa_+\omega_+^2}\frac{e^{-\pi\omega/\kappa_-}}{e^{2\pi\omega/\kappa_+}-1}|U|^2, \tag{20}$$

where we defined $\omega_+ = \omega + \omega'$, and:

$$U \equiv U\left(\frac{i\omega}{\kappa_-}, \frac{i\omega}{\kappa_S}, \frac{i\omega_+}{\bar{\kappa}}\right), \tag{21}$$

is a confluent hypergeometric Kummer function of the second kind, with $\kappa_S = 1/4M$ the usual surface gravity associated with the Schwarzschild event horizon. Here, $\bar{\kappa}^{-1} = 2(r_+ - r_-) = 4\psi = 4\sqrt{M^2 + l^2}$. This is analogous to the Kerr–Newman case with a replacement of the angular momentum and charge with the NUT parameter (with a sign difference between them; see Section 3 for a discussion of the rotating, charged scenario).

As shown in Figure 3, $N_{\omega\omega'}$ approaches thermality in the late-time regime, associated with $\omega' \gg \omega$ [8]. This limit describes the extreme Doppler shift experienced by the incoming plane wave modes, induced by the mirror trajectory. The main contribution to the Bogoliubov coefficients comes from these high-frequency modes. One can also demonstrate this thermal property analytically; that is,

$$\lim_{\omega'\gg\omega} N^{\mathrm{TN}}_{\omega\omega'} = N^{\mathrm{CW}}_{\omega\omega'} = \frac{1}{2\pi\kappa_+\omega'}\frac{1}{e^{2\pi\omega/\kappa_+}-1}, \tag{22}$$

which is also the eternal Planckian spectral form obtained for the Carlitz–Willey mirror trajectory [31] with temperature $T = \kappa_+/(2\pi)$ (i.e., associating $\kappa_+ \leftrightarrow \kappa$, where κ is the analog surface gravity of the eternal black hole).

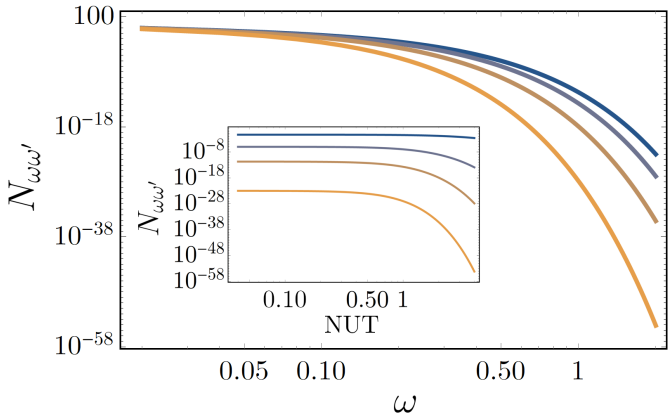

Figure 3. Mode-mode particle spectrum, Equation (20) emitted by the Taub-NUT (uncharged, non-rotating) analog mirror system, as a function of the outgoing frequency ω (main) and NUT parameter l (inset). In the main plot, we have used $l = 0, 1, 2, 4$ (dark blue to orange) while in the inset, $\omega = 0.1$, 0.5, 1, 2. In all cases, we have fixed $M = 1$ and $\omega' = 1$ for illustration.

It is also straightforward to verify that as the NUT parameter vanishes; the particle spectrum becomes:

$$\lim_{l\to 0} N^{\mathrm{TN}}_{\omega\omega'} = N^{\mathrm{S}}_{\omega\omega'} = \frac{\omega'}{2\pi\kappa_S\omega_+^2}\frac{1}{e^{2\pi\omega/\kappa_S}-1}, \tag{23}$$

which is the result found in [14] for the particle spectrum of the Schwarzschild analog mirror trajectory [32–34]. This limiting result, Equation (23), is valid for all times, not just late times, demonstrating the consistency of our approach with the canonical case.

From Figure 3, we also found that the introduction of the NUT parameter generally inhibits particle production, most clearly seen in the early-time limit (i.e., $\omega' \sim \omega$) in Figure 3. This is primarily due to the exponential suppression factor in Equation (20),

which, even for a small l, dramatically reduces $N_{\omega\omega'}$ by many orders of magnitude. From Equation (12), it can also be seen that the NUT parameter has a similar effect on the black hole surface gravity and, hence, the temperature and particle production, as the mass (i.e., heavier black holes radiate fewer particles). Since the temperature has an inverse square-root dependence on l—Equation (6)—, the particle production is likewise suppressed for larger l in the late-time thermal regime (however, this effect is barely visible in Figure 3).

3. Kerr–Newman Taub-NUT Mirror

Thus far, we considered a static, uncharged Taub-NUT spacetime and its analog mirror trajectory. Extension is warranted to the more general rotating, electrically charged Taub-NUT black hole. We note in passing that our analysis focused on the pure (analog) Hawking radiation emitted by the mirror–absent scattering effects [13]. A limitation of the accelerated boundary correspondence is the neglect of higher-dimensional effects; in the rotating scenario, this includes super-radiance, produced by incoming wave amplification due to the scattering off the rotating black hole. However, the influence of this effect primarily lies in the amplitude, rather than the frequency of the scattered modes. Hence, in the following, we restricted our focus to the s-wave pure (analog) Hawking radiation emitted.

3.1. Kerr–Newman Taub-NUT Metric

The Kerr–Newman Taub-NUT (KNTN) metric is given by:

$$\begin{aligned} \mathrm{d}s^2 = &-\frac{\Delta}{\rho^2}\left(\mathrm{d}t - P\mathrm{d}\phi\right)^2 + \frac{\rho^2}{\Delta}\left(\mathrm{d}r^2 + \Delta\mathrm{d}\theta^2\right) \\ &+ \frac{\sin^2\theta}{\rho^2}\left((r^2 + a^2 + l^2)\mathrm{d}\phi^2 - a\mathrm{d}t\right)^2, \end{aligned} \tag{24}$$

where

$$P = a\sin^2\theta - 2l\cos\theta, \tag{25}$$

$$\Delta = r^2 - 2Mr + a^2 + Q^2 - l^2, \tag{26}$$

$$\rho^2 = r^2 + (l + a\cos\theta)^2. \tag{27}$$

Here, $a = J/M$ is the mass-normalised angular momentum and Q is the charge. Following [16,17], we further restricted our analysis to a plane of constant θ, ϕ which yields the simplified (1+1)-dimensional metric:

$$\mathrm{d}s^2 = -f(r)\mathrm{d}t^2 + \frac{\mathrm{d}r^2}{f(r)}, \tag{28}$$

where

$$f(r) = \frac{r^2 - 2Mr + a^2 + Q^2 - l^2}{r^2 + (l + a\cos\theta)^2}. \tag{29}$$

From Equation (29), we found that the metric function, $f(r)$, is independent of ϕ; hence, the temperature of the Hawking radiation will likewise be unaffected by changes in ϕ. However, we also noticed the presence of the angular coordinate θ, which if left general, will leave an angular dependence in the temperature itself. To understand this, our model generated a correspondence between the (3+1)-dimensional black hole coordinates and the (1+1)-dimensional flat spacetime mirror trajectory by flattening out the two additional spatial dimensions defined by θ, ϕ. To date, this was achieved simply assuming a plane of constant θ, ϕ with arbitrary values, which has, likewise, yielded a valid tortoise coordinate which is independent of these parameters. However, the rotational degree of freedom in

the full KNTN metric, Equation (24), leads to the existence of an ergosphere outside the black hole defined by $r_+ < r < r_{e+}$, where:

$$r_{e+} = M + \sqrt{M^2 + l^2 - Q^2 - a^2 \cos^2\theta}. \tag{30}$$

Notice in particular that $r_{e+} = r_+$ (the outer horizon) when $\theta = 0$. In deriving the accelerated boundary correspondence between the black hole and the flat spacetime mirror trajectory, we required a tortoise coordinate defined with respect to the outer horizon, r_+, of the black hole. Thus, taking $\theta = 0$ yields a physically meaningful tortoise coordinate and, likewise, the correct outer horizon surface gravity. From this, we expected that the Hawking temperature of the outgoing radiation is the correct one, corresponding to that derived from other approaches, for example Equation (6). If $\theta \neq 0$, then one has an ill-defined tortoise coordinate which does not actually correspond to radial coordinate of the outer horizon.

With this in mind, we specialised to the plane of $\theta = 0$ and $\phi =$ const. which yields the tortoise coordinate:

$$r^\star = r + \frac{\gamma}{2\rho} \ln\left|\frac{r - r_+}{r - r_-}\right| + M \ln\left|\frac{(r - r_-)(r - r_+)}{r_S^2}\right|, \tag{31}$$

where we defined:

$$\gamma = 2al + 2l^2 + 2M^2 - Q^2, \tag{32}$$

$$\rho = \sqrt{M^2 + l^2 - a^2 - Q^2}. \tag{33}$$

The spacetime also possesses two horizons at the radial coordinates:

$$r_\pm = M \pm \sqrt{M^2 + l^2 - a^2 - Q^2}. \tag{34}$$

3.2. Kerr–Newman Taub-NUT Mirror

To obtain the exterior coordinate as a function of U, we performed the same matching condition analysis as before. The existence of two horizons for $r > 0$ allows for the choice of $v_0 - 2r_+ \equiv v_H$ or $v_0 - 2r_- \equiv v_H$, since $u \to \infty$ at $U = v_H$. When $l^2 < a^2 + Q^2$, the inner horizon, r_-, occurs at a $r > 0$, in contrast to the uncharged, non-rotating scenario. Without loss of generality, we set $v_H = 0$ and neglected the inner horizon solution so that $v_0 = 2r_+$. This choice is justified since it reduces to the correct Schwarzschild limit, wherein $r_- = 0$ represents the curvature singularity. Alternatively, one understands that the incoming modes are reflected off the centre of the black hole coordinate system, $r = 0$. The outer radius is chosen for the shell position since $r_+ > r_-$; the modes from the shell $v_0 = 2r_+$ will reach the observer at $\mathscr{I}_R^+$ first in both the mirror and black hole system, having already reflected off the mirror.

The exterior coordinate is then,

$$u(U) = U - \frac{1}{\kappa_+} \ln\left|\frac{U}{4M}\right| - \frac{1}{\kappa_-} \ln\left|\frac{U - 4\rho}{4M}\right|, \tag{35}$$

where the inverse surface gravities of the inner and outer horizons are given by:

$$\frac{1}{\kappa_\pm} = 2M \pm \frac{2al + 2l^2 + 2M^2 - Q^2}{\sqrt{M^2 + l^2 - a^2 - Q^2}}. \tag{36}$$

As before, we associated $u(U) \Leftrightarrow f(v)$ to obtain the trajectory of the mirror in (1+1)-dimensional Minkowski spacetime, given by:

$$f(v) = v - \frac{1}{\kappa_+} \ln\left|\kappa_S \nu\right| - \frac{1}{\kappa_-} \ln\left|\kappa_S (v - 4\rho)\right|. \tag{37}$$

The motion of the mirror is comparable to that found for the non-rotating, uncharged spacetime (see Figures 1 and 2); the parameters, M and Q, a only produce minor perturbations to the uncharged, non-rotating analog trajectory. The energy flux at late times is given by:

$$F(v) = \frac{\kappa_+^2}{48\pi} + \mathcal{O}(v^2), \tag{38}$$

which is constant, and dependent on M, Q, a and l.

As before, the mode–mode particle spectrum can be obtained via the Bogoliubov coefficients, and is given by:

$$N^{\mathrm{KNTN}}_{\omega\omega'} = \frac{\omega'}{2\pi\kappa_+\omega_+^2}\frac{e^{-\pi\omega/\kappa_-}}{e^{2\pi\omega/\kappa_+}-1}|U|^2, \tag{39}$$

where $\omega_+ = \omega + \omega'$ and again:

$$U \equiv U\left(\frac{i\omega}{\kappa_-}, \frac{i\omega}{\kappa_S}, \frac{i\omega_+}{\bar{\kappa}}\right) \tag{40}$$

is a confluent hypergeometric Kummer function of the second kind, where $\kappa_S = 1/(4M)$ as before. Here, $\bar{\kappa}^{-1} = 2(r_+ - r_-) = 4\sqrt{M^2 + l^2 - a^2 - Q^2}$, which reduces straightforwardly to the Kerr–Newman case as $l \to 0$, i.e., [17]:

$$\lim_{\omega' \gg \omega}\lim_{l\to 0} N^{\mathrm{KNTN}}_{\omega\omega'} = \lim_{\omega' \gg \omega} N^{\mathrm{KN}}_{\omega\omega'} = \frac{\omega'}{2\pi\kappa_+\omega_+^2}\frac{1}{e^{2\pi\omega/\kappa_+}-1} \tag{41}$$

(where the surface gravities are those of the Kerr–Newman case).

In general, the spectrum is similar to the Taub-NUT case shown in Figure 3 (hence, we left out a comparable graph for the KNTN case for brevity). In the high-frequency limit, the outgoing particle flux is thermal,

$$\lim_{\omega' \gg \omega} N^{\mathrm{KNTN}}_{\omega\omega'} = N^{\mathrm{CW}}_{\omega\omega'} = \frac{1}{2\pi\kappa_+\omega'}\frac{1}{e^{2\pi\omega/\kappa_+}-1}, \tag{42}$$

as expected. In the $l^2 - a^2 - Q^2 = 0$ limit, the results reduce to the familiar Schwarzschild case, e.g., [14].

To understand the dependence of particle production on the black hole parameters (Q, a, l), it is instructive to plot the early-time spectrum, as shown in Figure 4. This is because the early-time regime more explicitly unveils these dependences; the late-time regime yields the constant thermal production of the Carlitz-Willey trajectory. Figure 4 shows the early-time spectrum for the (a) Kerr Taub-NUT and (b) Reissner-Nordström Taub-NUT analog mirrors. In Figure 4a, we find that for Kerr Taub-NUT black holes, the NUT parameter inhibits particle production, and at a faster rate than an equal increase in the black hole's rotation. Interestingly for Reissner-Nordström Taub-NUT black holes – Figure 4b–the effect of the charge, Q, upon the radiated particle spectrum is nearly identical to that of the NUT parameter, l. That is, the early-time spectrum is nearly symmetric in Q, l. Further demonstration of the suppression of particle production by the presence of the NUT parameter is shown in Figure 5, which plots the early-time mode-mode spectrum of the Kerr-Newman Taub-NUT analog mirror. Figure 6 shows that the particle spectrum does not exhibit any special behaviour as $l^2 - a^2 - Q^2$ crosses from negative to positive values.

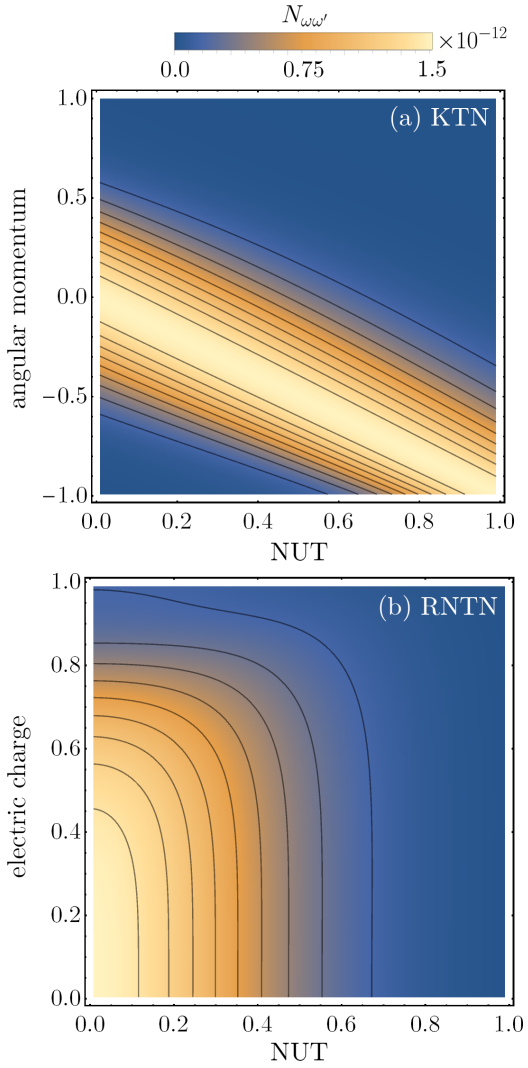

Figure 4. Mode-mode particle spectrum for the analog Kerr-Newman Taub-NUT mirror as a function (**a**) a, l with $Q = 0$ and (**b**) Q, l, with $a = 0$. In all plots, we have assumed an early-time regime, $\omega \sim \omega'$ (i.e. $\omega = \omega' = 1$).

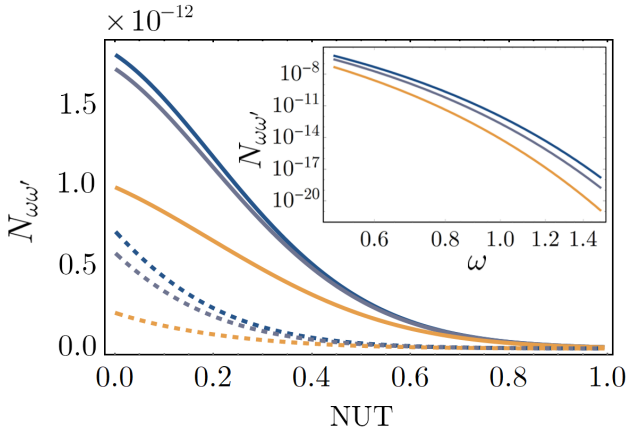

Figure 5. Mode-mode particle spectrum, Equation (39) for the Kerr-Newman Taub-NUT analog mirror. The main plot shows $N_{\omega\omega'}$ as a function of the NUT parameter, for different values of the charge; namely $Q = 0.1, 0.4, 0.7$ ranging from dark blue to orange, and the angular momentum, (solid) $a = 0.1$, and (dashed) $a = 0.7$. We have also taken $M = 1$ and the early-time limit, $\omega = \omega' = 1$. In the inset plot, $N_{\omega\omega'}$ is shown as a function of ω, for $l = 0.0, 0.5, 1.0$ with $M = \omega' = 1$, $a = 0.1$, $Q = 0.7$ fixed. Note in particular that the inset plot is shown on a log-log scale for clarity.

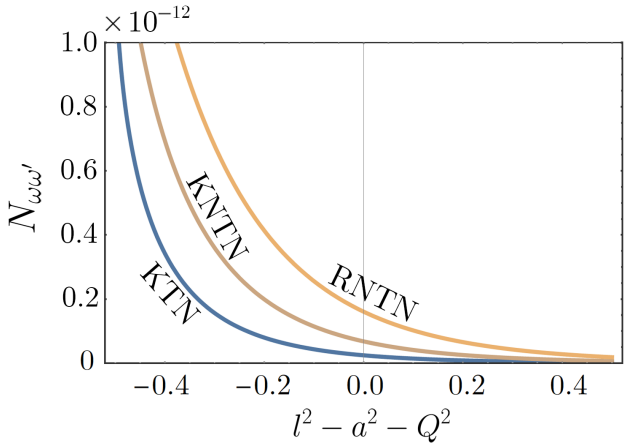

Figure 6. $N_{\omega\omega'}$ plotted against $l^2 - a^2 - Q^2$. The three lines correspond to (KNTN) $a = Q = 1/4$, (KTN) $a = 1/8$, $Q = 0$, and (RNTN) $a = 0$, $Q = 1/4$. We have also fixed $M = \omega = \omega' = 1$. Notably, $N_{\omega\omega'}$ exhibits no unusual behaviour as $l^2 - a^2 - Q^2$ crosses from negative to positive values. This behaviour occurs consistently across different incoming-outgoing frequency regimes.

4. Extremal Kerr–Newman Taub-NUT Mirror

The extremal limit occurs for $M^2 = a^2 + Q^2 - l^2$, describing the minimum possible mass compatible with the other free parameters which characterise the Kerr–Newman Taub-NUT black hole. Extremal black holes have been crucial in developing an understanding of the statistical origin of black hole entropy [35], making them relevant cases for studying quantum aspects of gravity.

In this limit, the metric function becomes:

$$f(r) = \frac{r^2 - 2\sqrt{a^2 + Q^2 - l^2}\, r + a^2 + Q^2 - l^2}{r^2 + (l + a)^2}, \tag{43}$$

taking the positive root of M. The tortoise coordinate is given by:

$$r^\star = r - \frac{2a(a + l) + Q^2}{r - M} + 2M \ln\left|\frac{r - M}{2M}\right|. \tag{44}$$

In Equation (44), we restored the mass parameter $M = +\sqrt{a^2 + Q^2 - l^2}$ where possible, bearing in mind that the extremal case is really characterised by three free parameters, rather than four. Performing the matching condition between the interior and exterior geometries of the black hole, we found that the exterior coordinate, as a function of U, is given by:

$$u(U) = U - \frac{4(2a(2a + l) + Q^2)}{U} - 4M \ln\left|\frac{U}{4M}\right|, \tag{45}$$

with the associated mirror trajectory given by:

$$f(v) = v - \frac{1}{\mathcal{A}^2 v} - \frac{1}{\kappa_S} \ln|\kappa_S v|, \tag{46}$$

where $\mathcal{A}$ is defined in Equation (48). The rapidity is:

$$\eta(v) = -\frac{1}{2} \ln\left|1 + \frac{1}{\mathcal{A}^2 v^2} - \frac{1}{\kappa_S v}\right|, \tag{47}$$

where we anticipated the introduction of the asymptotic uniform acceleration, $\mathcal{A}$, defined as:

$$\lim_{v \to 0^-} \alpha(v) = -\frac{1}{2\sqrt{2a^2 + 2al + Q^2}} \equiv -\mathcal{A}. \tag{48}$$

Using the usual definition for the total energy flux, one obtains the following expression for the energy flux as a function of v,

$$F(v) = \frac{\kappa_S^2 \mathcal{A}^6 v^3 \left(\mathcal{A}^2 v(1-4\kappa_S v) + 4\kappa_S(3\kappa_S v - 1)\right)}{48\pi(\mathcal{A}^2 v(\kappa_S v - 1) + \kappa_S)^4}. \tag{49}$$

As was found for the extremal Kerr-Newman analog mirror trajectory, the energy flux emitted by the extremal Kerr-Newman Taub-NUT mirror, Figure 7a, vanishes at late times, $v \to 0$, and reduces to the result derived in [17] as $l \to 0$.

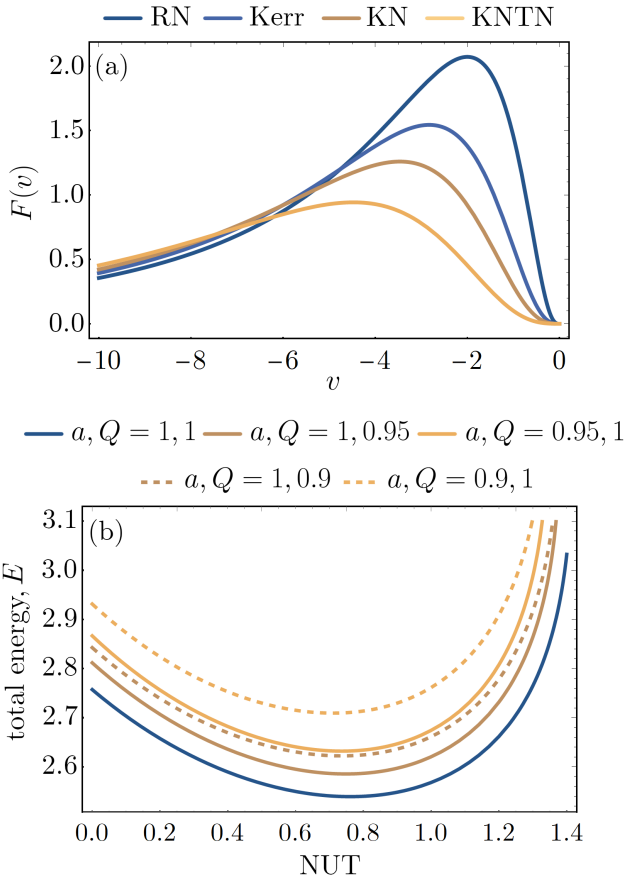

Figure 7. (**a**) Time-dependent energy flux, $F(v)$ (normalised by 10^{-4}), plotted as a function of v for the different extremal black hole solutions. The values of a, Q, l are either 0 or $+1$, corresponding to the relevant solution. (**b**) The total energy (normalised by 10^{-3}) emitted by the KNTN black hole as a function of the NUT parameter.

The total energy radiated by the mirror is given by:

$$\begin{aligned} E &= \int_{-\infty}^{v_H=0} F(v) \frac{\mathrm{d}f(v)}{\mathrm{d}v} \mathrm{d}v \\ &= -\frac{\mathcal{A}\kappa_S}{48\pi\zeta^3}\left[\mathcal{A}\zeta + \mu\left(\pi - 2\tan^{-1}\left(\frac{\mathcal{A}}{\zeta}\right)\right)\right], \end{aligned} \tag{50}$$

with

$$\zeta = \sqrt{4\kappa_S^2 - \mathcal{A}^2}, \tag{51}$$

$$\mu = \mathcal{A}^2 - 6\kappa_S^2. \tag{52}$$

Analogous to other recent extremal black hole results (Kerr, Reissner–Nordström and Kerr–Newman mirrors), we found that the total energy radiated by the extremal Kerr–

Newman Taub-NUT mirror is finite and reduces to the appropriate limits for a vanishing NUT parameter.

In Figure 7b, we have plotted the total energy radiated by the mirror as a function of the NUT parameter. Intriguingly, for small l, the energy decreases, before increasing as $l \to \sqrt{a^2 + Q^2}$ – that is, in the limit where the mass of the extremal black hole vanishes. It has been conjectured that tiny mass black holes were present in high densities in the early universe [36]. The effect of this dominant energy contribution from primordial (i.e. tiny mass) Taub-NUT black holes upon the evolution of matter and energy densities in the early universe would be an interesting problem to pursue in future studies.

In Figure 8a, we have plotted the total energy emitted by the mirror as a function of the angular momentum parameter, a. In general, we see that the total energy decays with increasing a, which corresponds to an increasing extremal black hole mass. Notably, we find that for small values of a, the presence of a non-zero (and larger) NUT parameter amplifies the total energy. This result corroborates the findings of Figure 7b. At a threshold value of a, the energy of the $l = 0$ mirror (i.e. the extremal Kerr-Newman analog) intersects that of the $l \neq 0$ mirrors; above this threshold, the presence of the NUT charge inhibits the total energy radiated compared with the $l = 0$ case.

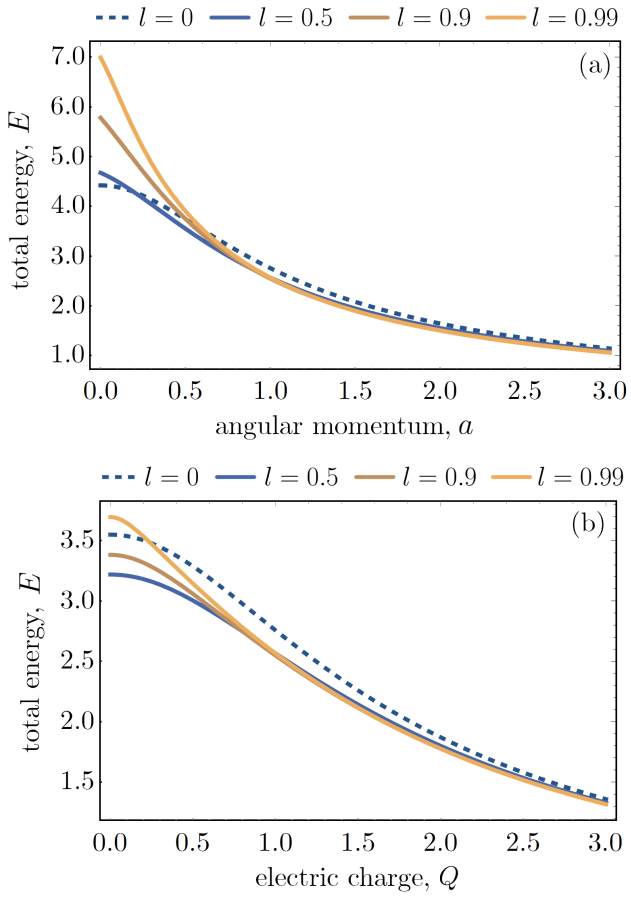

Figure 8. (**a**) Total energy, E, radiated by the extremal KNTN mirror as a function of the angular momentum for different values of the NUT parameter, with $Q = 1$ fixed. (**b**) Total energy, E, as a function of the charge, Q, with $a = 1$ fixed. Both plots have been normalised by 10^{-3}.

In Figure 8b, we have plotted the total energy emitted by the mirror as a function of the charge, Q, with fixed a and different values of l. The plot complements Figure 8a, which shows that there is a specific value of l for each set of (Q, a) which minimizes the total energy radiated.

To derive the mode–mode particle spectrum, $N_{\omega\omega'}$, we performed the usual procedure and calculated the Bogoliubov coefficients between the incoming and outgoing modes. Performing this calculation yields,

$$N^{\text{KNTN}}_{\omega\omega'} := \left|\beta^{\text{KNTN}}_{\omega\omega'}\right|^2 = \frac{e^{-\pi\omega/\kappa_S}\omega'}{\pi^2\mathcal{A}^2\omega_+}\left|K_n\left(\frac{2}{\mathcal{A}}\sqrt{\omega\omega_+}\right)\right|^2 \tag{53}$$

where $K_n(x)$ is the modified Bessel function of the second kind, where $n = 1 - i\omega/\kappa_S$, and we defined $\omega_+ = \omega + \omega'$. This spectrum is characteristically non-thermal, and accords with the results found in [17,37] in the appropriate limits. It is important to note that the corresponding trajectory dynamics of the analog extremal mirror completely differ from the non-extremal case. This reflects the uniqueness of extremal black hole solutions, which possess vanishing surface gravity and, hence, an undefined temperature. Likewise, the non-thermal particle spectrum, Equation (53), should not be considered to be a limiting case of the non-extremal spectrum.

In Figure 9, we plotted the early-time particle spectrum, $N_{\omega\omega'}$, for the extremal Kerr–Newman Taub-NUT analog mirror, as a function of the NUT parameter, l. We discovered that the particle spectrum initially *decreases* with increasing l (i.e., as the mass of the extremal black hole *decreases*). As the mass approaches zero, the particle number begins to increase and diverges as $l \to \sqrt{a^2 + Q^2}$. In the late-time regime, $\omega' \gg \omega$, the radiation exhibits similar behaviour. One can understand this as a competition between the increasing NUT parameter (which we found for non-extremal black holes, inhibits particle production) with a decreasing black hole mass (which typically makes non-extremal black holes hotter; of course, here, we could not meaningfully assign a temperature to the radiation, since it is non-thermal). The particle spectrum Equation (53) is in agreement with the energy flux of the quantum stress tensor, Equation (49). Numerical checks confirm that the method of quantum summing,

$$E = \int_0^\infty \int_0^\infty \omega\, N^{\text{KNTN}}_{\omega\omega'}\, \mathrm{d}\omega\, \mathrm{d}\omega', \tag{54}$$

yields the total energy Equation (50), confirming the mathematical consistency of the spectral results. The physical interpretation is that the particles carry the energy; we concluded that the non-monotonic effect on the particle radiation as a function of the NUT parameter is a reliable result.

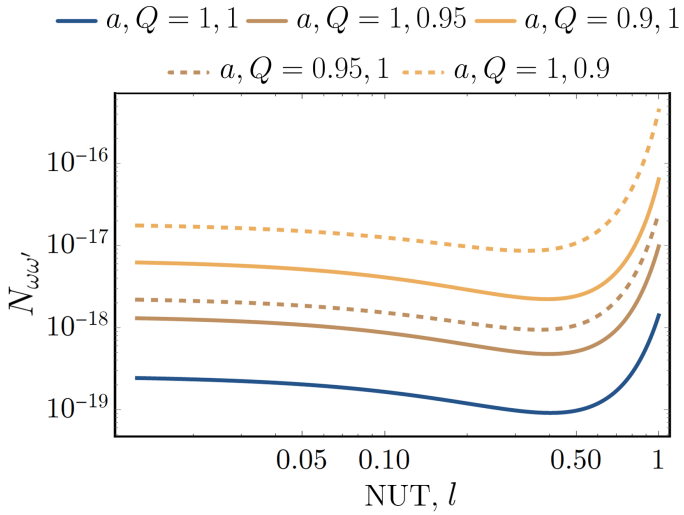

Figure 9. Log-log plot of the particle spectrum, $N_{\omega\omega'}$, radiated by the extremal KNTN mirror as a function of the NUT parameter, l. We have taken $\omega = \omega' = 1$, however we also verified that the non-monotonicity is robust to arbitrary choices of ω, ω'.

5. Conclusions

In this paper, we investigated an accelerated boundary correspondence which mimics the outgoing Hawking radiation produced by a general class of Taub-NUT black holes. The solution is thermal at late times, approaching the Schwarzschild and Carlitz–Willey limits in the appropriate regimes. In the rotating, electrically charged case, we found that the presence of the NUT parameter, l, generally suppresses particle production. Moreover, we found no indication that the ABC form of the Hawking radiation spectrum responds to the type of singularity in the Taub-NUT metric that results in an absence of global asymptotic flatness. The extremal Kerr–Newman Taub-NUT case is a particularly interesting result, whereby the particle and energy spectrum are shown to be non-monotonic as a function of the NUT parameter, in contrast to the non-extremal case.

As in other recent works, the aim of this paper was to communicate the utility of the ABC method in extracting physically meaningful insights into the Hawking radiation properties of different kinds of black holes. This approach has the advantage of yielding analytic expressions for quantities such as the particle spectrum and energy flux. We envision it will continue to be utilised as a tool for analysing complex and exotic cosmological spacetimes.

Author Contributions: All authors contributed equally to this work. All authors have read and agreed to the published version of the manuscript

Funding: J.F. acknowledges support from the Australian Research Council Centre of Excellence for Quantum Computation and Communication Technology (project no. CE170100012). M.G. was funded from the state-targeted program the "Center of Excellence for Fundamental and Applied Physics" (BR05236454) by the Ministry of Education and Science of the Republic of Kazakhstan. M.G. was also funded by the FY2021-SGP-1-STMM Faculty Development Competitive Research grant no. 021220FD3951 at Nazarbaev University. R.B.M. acknowledges support from the Natural Sciences and Engineering Research Council of Canada.

Conflicts of Interest: The authors declare no conflict of interest. The funders had no role in the design of the study; in the collection, analyses, or interpretation of data; in the writing of the manuscript, or in the decision to publish the results.

Appendix A. Vanishing Two-Space Curvature ($\varepsilon = 0$)

In our prior analysis, we assumed a NUT solution with a positive two-space curvature, $\varepsilon = 1$. More generally, the line element takes the form:

$$\begin{aligned} \mathrm{d}s^2 = &-f(r)\left[\mathrm{d}t + \frac{il\left(\zeta \mathrm{d}\bar{\zeta} - \bar{\zeta}\mathrm{d}\zeta\right)}{1+\varepsilon\zeta\bar{\zeta}/2}\right]^2 + \frac{\mathrm{d}r^2}{f(r)} \\ &+ (r^2+l^2)\frac{2\mathrm{d}\zeta\mathrm{d}\bar{\zeta}}{(1+\varepsilon\zeta\bar{\zeta}/2)^2}, \end{aligned} \tag{A1}$$

where

$$f(r) = \frac{\varepsilon(r^2-l^2)-2Mr}{r^2+l^2}, \tag{A2}$$

and ε is the discrete, two-space curvature which takes on the values $\varepsilon \in \{-1, 0, 1\}$. When $\varepsilon = +1$, one can set $\zeta = \sqrt{2}\tan(\theta/2)e^{i\phi}$ and the line element reduces to the form of Equation (3). In the following, we studied the $\varepsilon = 0$ case, which corresponds to a new class of mirror trajectories possessing an early-time thermal spectrum.

Appendix B. Taub-NUT Mirror ($\varepsilon = 0$)

For $\varepsilon = 0$, the metric is:

$$\mathrm{d}s^2 = -f(r)\left(\mathrm{d}t + l\rho^2\mathrm{d}\phi\right)^2 + \frac{\mathrm{d}r^2}{f(r)} + (r^2+l^2)\mathrm{d}\Theta^2, \tag{A3}$$

where

$$f(r) = -\frac{2Mr}{r^2 + l^2} \tag{A4}$$

and $\mathrm{d}\Theta^2 = \mathrm{d}\rho^2 + \rho^2 \mathrm{d}\phi^2$. To obtain Equation (A3), we set $\zeta = \rho e^{i\phi}/\sqrt{2}$ in Equation (A1); in Equation (A1), $\rho = 0$ behaves such as an axis for which ϕ is the associated periodic coordinate [20]. Conformal diagrams for sections of the maximally extended spaces with metric Equation (A3) were given by Siklos [38]. These correspond to the two-space with $\rho, \phi =$ const., yielding the line element:

$$\mathrm{d}s^2 = \frac{2Mr}{r^2 + l^2}\mathrm{d}t^2 - \frac{r^2 + l^2}{2Mr}\mathrm{d}r^2. \tag{A5}$$

In this section, we derived the accelerated boundary correspondence for Equation (A5). Notice that the surfaces of constant r have time-like normals for $r < 0$ and space-like normals for $r > 0$. The usual ansatz assumed in the accelerated mirror model is that $r > 0$, which accords with the regularity condition imposed on incoming modes. That is, the reflecting point of the modes is the $r = 0$ centre of the black hole itself. Such a system (i.e., with time-like r) has not been studied in the context of accelerating mirrors and, hence, the physical interpretation is not entirely clear. Curiously, if one makes the simple replacement $r \to -r$ (so that r becomes the usual space-like radial quantity), yielding the metric:

$$\mathrm{d}s^2 = -\frac{2Mr}{r^2 + l^2}\mathrm{d}t^2 + \frac{r^2 + l^2}{2Mr}\mathrm{d}r^2 \tag{A6}$$

the corresponding mirror trajectory becomes space-like (admits faster-than-light trajectories), which is unphysical.

Furthermore, adopting Equation (A5) as stated leads to a valid spacetime trajectory possessing an *early-time* acceleration horizon, i.e., begins light-like in the asymptotic past (see the trajectory diagrams in Figures A1 and A2). Hence, we expected the spectrum to be thermal at early times, rather than at late times as is usually the case for mirrors which approach the speed of light with an acceleration horizon in the asymptotic future. Tentatively, we suggest that the reversal in the sign of the time coordinate in the metric leads to an overall time reversal in the usual particle production dynamics of the mirror trajectory, leading to the early-time thermal result (as we derived below). Therefore, this mirror trajectory, and the ensuing spectrum, cannot have a direct physical correspondence to the behaviour of a typical black hole formed via a gravitational collapse. Nevertheless, we are interested in the effects induced by this new class of mirror trajectories, which, as we demonstrated, yield an entirely new particle and energy spectrum. Note that, despite the swapped roles of t and r *at the level of the metric* (A3), once we determined the relevant associations between $u(U)$ and the flat spacetime trajectory $f(v)$, these details are flattened out; t and z take on their usual interpretations and temporal and spatial coordinates.

For the $\varepsilon = 0$ metric, the horizon occurred at $r = 0$ and is asymptotically flat as $r \to \pm\infty$. As mentioned, we considered $r \geq 0$, where, as usual, $r = 0$ functions as the reflecting point of incoming modes.

As before, we specialised to (1+1)-dimensions by considering a plane where $\theta = \phi =$ const., so that:

$$\mathrm{d}s^2 = -f(r)\mathrm{d}t^2 + \frac{\mathrm{d}r^2}{f(r)}. \tag{A7}$$

The tortoise coordinate (which is really a temporal tortoise coordinate [39]) is:

$$r^\star = -\frac{r^2}{4M} - \frac{l^2}{2M}\ln\left|\frac{r}{r_S^2}\right|, \tag{A8}$$

where we included an appropriately chosen integration constant in the denominator of the logarithm. Note that swapping $r \to -r$ at the level of the tortoise coordinate does not actually change $r^\star$; hence, the mirror trajectory remains identical. Furthermore, $r^\star \to +\infty$

as $r \to 0^+$. As before, we applied the usual matching condition to the exterior (u) and interior (U) coordinates. Noting the single horizon at $r = 0$ and taking $v_0 = 0$ without the loss of generality, we obtained:

$$u(U) = \frac{U^2}{8M} + \frac{l^2}{M} \ln \left| \frac{U}{2r_S^2} \right|. \tag{A9}$$

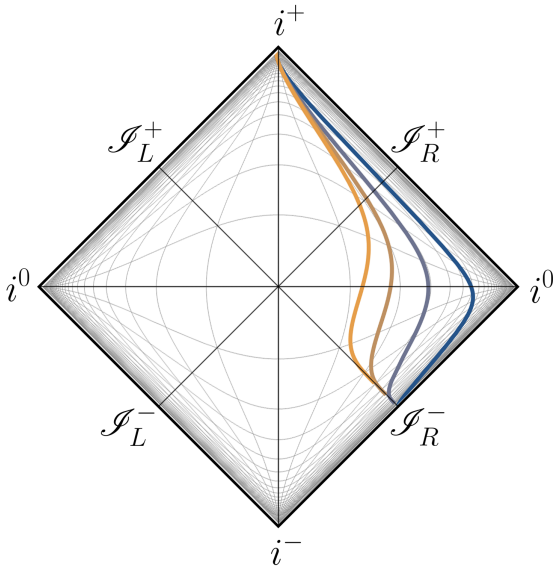

Figure A1. Conformal Penrose diagram for the analog Taub-NUT mirror trajectory, with vanishing 2-space curvature $\varepsilon = 0$. The trajectories shown correspond to $l = 0.5, 1.0, 1.5, 2.0$, from dark blue to orange.

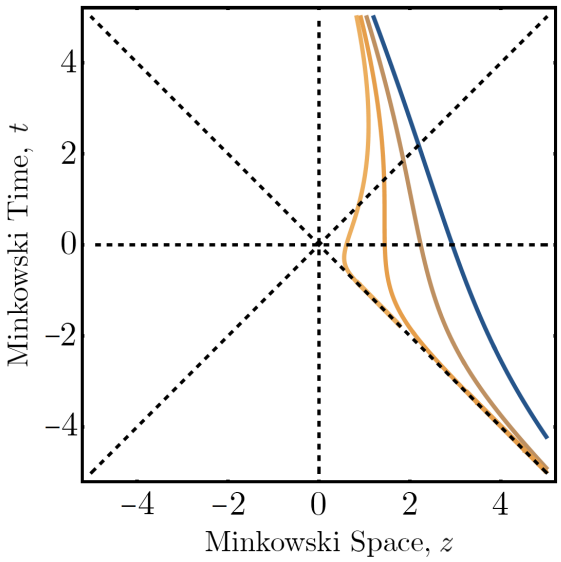

Figure A2. Corresponding spacetime trajectories for the Taub-NUT analog mirror, clearly illustrating the early-time horizon. We have used the same settings as Figure A1.

The mirror trajectory can be obtained by associating $u(U) = f(v)$ so that:

$$f(v) = \frac{\kappa_S v^2}{2} + \frac{1}{\kappa} \ln \left| \frac{v}{2r_S^2} \right| \tag{A10}$$

where κ_S is the usual Schwarzschild surface gravity and $\kappa = M/l^2$. We note here that the trajectory Equation (A10) represents a novel class of mirror trajectories that has not yet been studied. The rapidity is:

$$\eta(v) = -\frac{1}{2}\ln\left|\frac{1}{\kappa v} + \kappa_S v\right|. \tag{A11}$$

The mirror is asymptotically null in the infinite past and future, as shown in Figure A1. In Figure A2, we saw that the trajectories diverge from null infinity, $\mathcal{I}_R^-$, and converge to time-like future infinity i^+. That is, even though both asymptotic regimes approach the speed of light, only the early-time regime possesses a null horizon. The late-time regime is asymptotically inertial.

One can also obtain the proper acceleration, which to the leading order in v near $v \to 0^-$ is:

$$\alpha(v) = -\frac{\sqrt{\kappa_S v}}{2\kappa_S v^2} + \mathcal{O}(v^3). \tag{A12}$$

In the asymptotic past, the mirror possesses infinite acceleration (in the direction opposite to its motion) and coasts at the speed of light in the asymptotic future (and, hence, does not possess an acceleration horizon). As long as acceleration is asymptotically zero, even in the presence of a divergent rapidity (the mirror attains the speed of light), the mirror will be asymptotically inertial and its evolution will be toward an asymptotic drift at a constant velocity. Coasting trajectories [30,40–44] have been studied as models for black hole remnants [45].

Appendix C. Energy Flux and Particle Spectrum ($\varepsilon = 0$)

The time-dependent energy flux, calculated using the usual Schwarzian derivative, is given by:

$$F(v) = \frac{\kappa^2}{48\pi}\left[\frac{1 + 10\kappa\kappa_S v^2 - 3\kappa^2\kappa_S^2 v^4}{(1+\kappa\kappa_S v^2)^4}\right]. \tag{A13}$$

At early times $v \to 0^+$, the energy flux to the leading order in v is constant, and given by:

$$F(v) = \frac{\kappa^2}{48\pi} + \mathcal{O}(v^2). \tag{A14}$$

The constancy of $F(v)$ at early times is indicative of thermality, which is corroborated by the early-time spectrum for the particle production of the mirror, discussed below. Meanwhile for late times, $v \to \infty$, the energy flux is negative and asymptotes to zero from below,

$$F(v) = -\frac{1}{16\pi\kappa_S^2 v^4} + \mathcal{O}(\lambda^5). \tag{A15}$$

Figure A3 displays the energy flux, $F(v)$, as a function of the advanced time coordinate v. The spectrum possesses two turning points at finite v, occurring at:

$$v_\pm = \sqrt{\frac{3 \pm 2\sqrt{2}}{\kappa\kappa_S}}. \tag{A16}$$

After the initial burst of thermal particles, the flux increases towards a maximum at v_+, before decreasing and becoming negative and reaching a minimum at v_-. After this point, the energy emitted is negative into the asymptotic future. Negative energy emission from accelerated mirrors has been studied in [46–51] and, more pertinently, has been shown in settings where the trajectories are asymptotically coasting [52,53]. The unitary evolution of conformal black holes evaporating non-monotonically require some

transient period of a negative energy flux [54,55]. The presence of a negative energy flux can also be understood in terms of outgoing modes whose quadratures are squeezed below the quantum shot-noise limit [56]. Note that as we already mentioned, our results for the trajectory dynamics of the mirror and the corresponding particle and energy production made sense as a black hole analogy when time runs backwards.

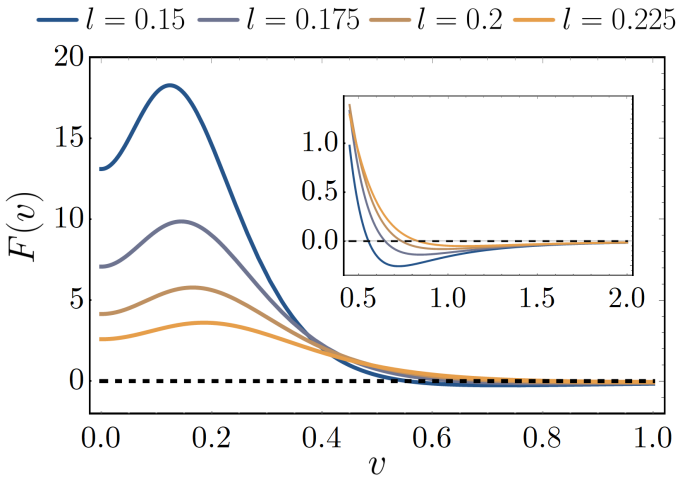

Figure A3. A plot of the energy flux as a function of the advanced time, with $M = 1$ fixed. The inset shows the region of negative energy flux.

We could also calculate the Bogoliubov coefficients and, hence, the particle spectrum, analytically. The Bogoliubov coefficients are:

$$\beta_{\omega\omega'} = \frac{1}{2\pi}\sqrt{\frac{\omega'}{\omega}}\int_0^\infty \mathrm{d}v\, e^{-i\omega' v - i\omega f(v)} \tag{A17}$$

noting that the integration domain is now $v \in [0, \infty)$. The particle number is given by:

$$N^{(\varepsilon=0)}_{\omega\omega'} := \left|\beta_{\omega\omega'}\right|^2 = \frac{\omega' e^{-\pi\omega/2\kappa}}{8\pi^2\kappa_S^2\omega^3}|\mathcal{F}|^2 \tag{A18}$$

where $\mathcal{F} \equiv \mathcal{F}(\omega, \omega')$ is defined as:

$$\begin{aligned}\mathcal{F} = {} & i\sqrt{i\kappa_S\omega}\,\Gamma\left(\frac{\kappa - i\omega}{2\kappa}\right){}_1F_1\left(\frac{\kappa - i\omega}{2\kappa}, \frac{1}{2}, \frac{i\omega'^2}{2\kappa_S\omega}\right) \\ & + \sqrt{2}\omega'\Gamma\left(1 - \frac{i\omega}{2\kappa}\right){}_1F_1\left(1 - \frac{i\omega}{2\kappa}, \frac{3}{2}, \frac{i\omega'^2}{2\kappa_S\omega}\right)\end{aligned} \tag{A19}$$

and ${}_1F_1(a, b, z)$ are confluent hypergeometric functions of the first kind, and $\Gamma(z)$ is the Gamma function. The result Equation (A18) has radiated particles in a Planck distribution at early times to an observer on the right $\mathscr{I}_R^+$,

$$\lim_{\omega' \gg \omega} N^{(\varepsilon=0)}_{\omega\omega'} = N^{\mathrm{CW}}_{\omega\omega'} = \frac{1}{2\pi\kappa\omega'}\frac{1}{e^{2\pi\omega/\kappa} - 1}, \tag{A20}$$

which can be found by the usual Hawking approximation [8] $\omega' \gg \omega$ on Equation (A18). This limit is complementary to the *late-time* approximation taken for a mirror starting the past time-like infinity and receding to $\mathscr{I}_L^+$, for example, the $\varepsilon = +1$ trajectory. Since there is a steady-state energy flux emitted at early times, Equation (A14), one can see by using Equation (A20) that the particles have temperature at $T = \kappa/(2\pi)$ at asymptotic early retarded times.

Figure A4 displays the mode–mode particle spectrum of the mirror for increasing (from dark blue to orange) values of the NUT parameter. From the values of l for which we plotted $N_{\omega\omega'}$, one might naively conclude that particle production is generally inhibited

for larger NUT parameters. However we discovered that $N_{\omega\omega'}$ is actually a non-monotonic function of the NUT parameter, as displayed in Figure A5. The dashed lines correspond to the $\varepsilon = +1$ particle number, which decays monotonically with l, for all values of M, ω and ω'.

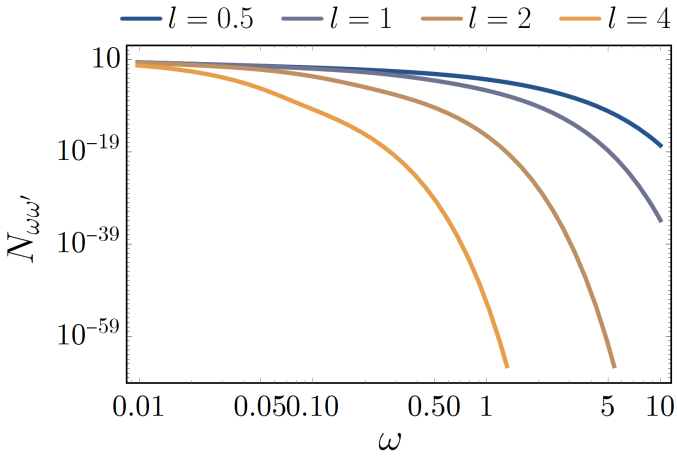

Figure A4. Mode-mode particle spectrum, Equation (A18), for the Taub-NUT ($\varepsilon = 0$) analog mirror as a function of ω with $\omega' = 1$ fixed with $M = 1$ fixed.

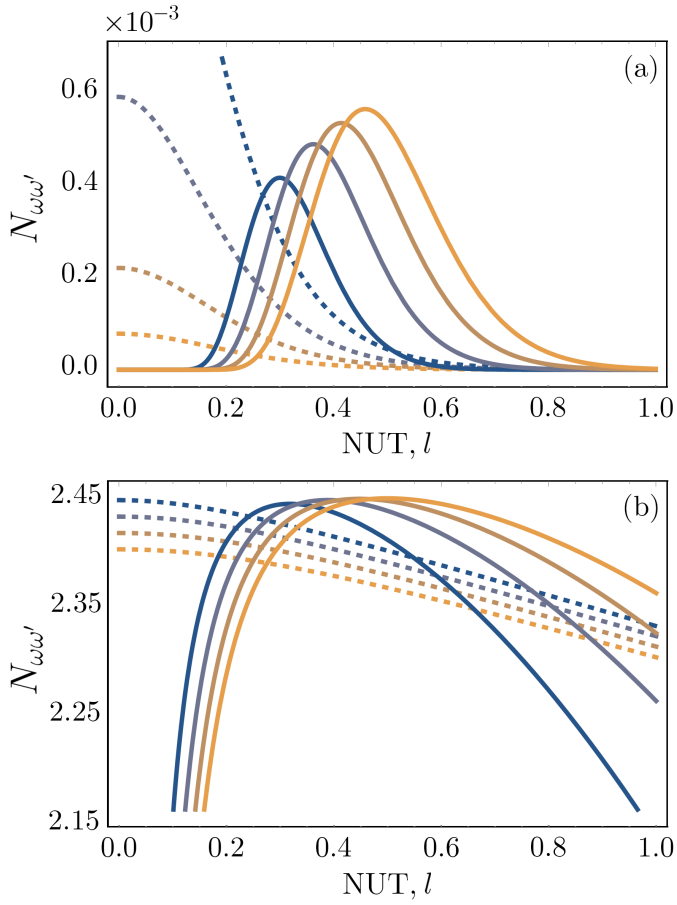

Figure A5. Plot of the particle number as a function of the NUT parameter, l, for different values of M. We have used (**a**) $\omega = 1$ and (**b**) $\omega = 0.01$, with $\omega' = 1$ in both plots. The dashed lines correspond to $N_{\omega\omega'}$ for the $\varepsilon = +1$ mirror, while the solid lines represent $N_{\omega\omega'}$ for the $\varepsilon = 0$ mirror. The colours (dark blue to orange) represent different black hole masses, $M = 0.1, 0.15, 0.2, 0.25$ respectively.

The solid lines, corresponding to $\varepsilon = 0$, show that the particle number vanishes in the limit of small l, a limit which was also verified analytically. For intermediate values of l, the particle number grows towards a maximum, the peak value of which depends on the mass of the black hole. Beyond this peak, the particle number decays to zero for large values of l. This behaviour is present for both the $\omega \sim \omega'$ and $\omega \ll \omega'$ regimes.

The results shown in this Appendix were motivated by the existence of a viable mirror trajectory obtained by the usual method from the metric of the $\varepsilon = 0$ Taub-NUT black hole. Our interest in this solution is primarily in the features of the derived mirror trajectory. The extent to which our result connects with the properties of a physical black hole remains an interesting direction for future research. Moreover, it would be interesting to study other systems in which t and r swap roles, and whether corresponding mirror trajectories generally give such a behaviour.

References

1. Taub, A. Empty space-times admitting a three parameter group of motions. *Ann. Math.* **1951**, *53*, 472–490. [CrossRef]
2. Newman, E.; Tamburino, L.; Unti, T. Empty space generalization of the Schwarzschild metric. *J. Math. Phys.* **1963**, *4*, 915. [CrossRef]
3. Hawking, S.; Hunter, C.; Page, D.N. Nut charge, anti-de Sitter space and entropy. *Phys. Rev. D* **1999**, *59*, 044033. [CrossRef]
4. Chamblin, A.; Emparan, R.; Johnson, C.V.; Myers, R.C. Large N phases, gravitational instantons and the nuts and bolts of AdS holography. *Phys. Rev. D* **1999**, *59*, 064010. [CrossRef]
5. Emparan, R.; Johnson, C.V.; Myers, R.C. Surface terms as counterterms in the AdS/CFT correspondence. *Phys. Rev. D* **1999**, *60*, 104001. [CrossRef]
6. Mann, R.B. Misner string entropy. *Phys. Rev. D* **1999**, *60*, 104047. [CrossRef]
7. Kerr, R.P. Gravitational field of a spinning mass as an example of algebraically special metrics. *Phys. Rev. Lett.* **1963**, *11*, 237–238. [CrossRef]
8. Hawking, S. Particle Creation by Black Holes. *Commun. Math. Phys.* **1975**, *43*, 199–220. [CrossRef]
9. Fulling, S.A.; Davies, P.C.W. Radiation from a moving mirror in two dimensional space-time: Conformal anomaly. *Proc. R. Soc. Lond. A Math. Phys. Sci.* **1976**, *348*, 393–414.
10. Davies, P.; Fulling, S. Radiation from Moving Mirrors and from Black Holes. *Proc. R. Soc. Lond. A Math. Phys. Sci.* **1977**, *A356*, 237–257. [CrossRef]
11. DeWitt, B.S. Quantum Field Theory in Curved Space-Time. *Phys. Rep.* **1975**, *19*, 295–357. [CrossRef]
12. Birrell, N.; Davies, P. *Quantum Fields in Curved Space*; Cambridge Monographs on Mathematical Physics; Cambridge University Press: Cambridge, UK, 1984; [CrossRef]
13. Fabbri, A.; Navarro-Salas, J. *Modeling Black Hole Evaporation*; Imperial College Press: London, UK , 2005.
14. Good, M.R.R.; Anderson, P.R.; Evans, C.R. Mirror Reflections of a Black Hole. *Phys. Rev. D* **2016**, *94*, 065010. [CrossRef]
15. Good, M.R.R.; Ong, Y.C. Particle spectrum of the Reissner-Nordström black hole. *arXiv* **2020**, arXiv:gr-qc/2004.03916.
16. Good, M.R.; Foo, J.; Linder, E.V. Accelerating boundary analog of a Kerr black hole. *arXiv* **2020**, arXiv:gr-qc/2006.01349.
17. Foo, J.; Good, M.R. Hawking radiation particle spectrum of a Kerr–Newman black hole. *arXiv* **2020**, arXiv:gr-qc/2006.09681.
18. Kerner, R.; Mann, R.B. Tunnelling, temperature and Taub-NUT black holes. *Phys. Rev. D* **2006**, *73*, 104010, [CrossRef]
19. Al-Badawi, A.; Halilsoy, M. On the physical meaning of the NUT parameter. *Gen. Relativ. Gravit.* **2006**, *38*, 1729–1734. [CrossRef]
20. Griffiths, J.B.; Podolskỳ, J. *Exact Space-Times in Einstein's General Relativity*; Cambridge University Press: Cambridge, UK, 2009; [CrossRef]
21. Misner, C.W. The Flatter regions of Newman, Unti and Tamburino's generalized Schwarzschild space. *J. Math. Phys.* **1963**, *4*, 924–938. [CrossRef]
22. Hajicek, P. Causality in non-Hausdorff space-times. *Commun. Math. Phys.* **1971**, *21*, 75–84. [CrossRef]
23. Clément, G.; Gal'tsov, D.; Guenouche, M. Rehabilitating space-times with NUTs. *Phys. Lett. B* **2015**, *750*, 591–594. [CrossRef]
24. Clément, G.; Gal'tsov, D.; Guenouche, M. NUT wormholes. *Phys. Rev. D* **2016**, *93*, 024048. [CrossRef]
25. Miller, J.; Kruskal, M.; Godfrey, B.B. Taub-NUT (Newman, Unti, Tamburino) Metric and Incompatible Extensions. *Phys. Rev. D* **1971**, *4*, 2945–2948. [CrossRef]
26. Hennigar, R.A.; Kubizňák, D.; Mann, R.B. Thermodynamics of Lorentzian Taub-NUT spacetimes. *Phys. Rev. D* **2019**, *100*, 064055. [CrossRef]
27. Bordo, A.B.; Gray, F.; Kubizňák, D. Thermodynamics and Phase Transitions of NUTty Dyons. *J. High Energy Phys.* **2019**, *2019*, 119. [CrossRef]
28. Ballon Bordo, A.; Gray, F.; Kubizňák, D. Thermodynamics of Rotating NUTty Dyons. *J. High Energy Phys.* **2020**, *2020*, 84, [CrossRef]
29. Ballon Bordo, A.; Gray, F.; Hennigar, R.A.; Kubizňák, D. The First Law for Rotating NUTs. *Phys. Lett. B* **2019**, *798*, 134972. [CrossRef]

30. Good, M.R.R.; Yelshibekov, K.; Ong, Y.C. On Horizonless Temperature with an Accelerating Mirror. *J. High Energy Phys.* **2017**, *2017*, 13. [CrossRef]
31. Carlitz, R.D.; Willey, R.S. Reflections on moving mirrors. *Phys. Rev. D* **1987**, *36*, 2327–2335. [CrossRef]
32. Good, M.R.R. Reflections on a Black Mirror. In *Everything about Gravity: Proceedings of the Second LeCosPA International Symposium*; World Scientific: Singapore, 2017; pp. 560–565. [CrossRef]
33. Anderson, P.R.; Good, M.R.R.; Evans, C.R. Black hole—Moving mirror I: An exact correspondence. In *The Fourteenth Marcel Grossmann Meeting*; World Scientific: Singapore, 2017; pp. 1701–1704. [CrossRef]
34. Good, M.R.R.; Anderson, P.R.; Evans, C.R. Black hole—Moving mirror II: Particle creation. In *The Fourteenth Marcel Grossmann Meeting*; World Scientific: Singapore, 2017; pp. 1705–1708. [CrossRef]
35. Strominger, A.; Vafa, C. Microscopic origin of the Bekenstein-Hawking entropy. *Phys. Lett. B* **1996**, *379*, 99–104. [CrossRef]
36. Zel'dovich, Y.B.; Novikov, I.D. The hypothesis of cores retarded during expansion and the hot cosmological model. *Soviet Astronomy* **1967**, *10*, 602.
37. Good, M.R.R.; Zhakenuly, A.; Linder, E.V. Mirror at the edge of the universe: Reflections on an accelerated boundary correspondence with de Sitter cosmology. *Phys. Rev. D* **2020**, *102*, 045020. [CrossRef]
38. Siklos, S. Two completely singularity-free NUT spacetimes. *Phys. Lett. A* **1976**, *59*, 173–174. [CrossRef]
39. Batic, D.; Nicolini, P. Fuzziness at the horizon. *Phys. Lett. B* **2010**, *692*, 32–35. [CrossRef]
40. Good, M.R.; Ong, Y.C.; Myrzakul, A.; Yelshibekov, K. Information preservation for null shell collapse: A moving mirror model. *Gen. Relativ. Gravit.* **2019**, *51*, 92. [CrossRef]
41. Good, M.R. Spacetime Continuity and Quantum Information Loss. *Universe* **2018**, *4*, 122. [CrossRef]
42. Myrzakul, A.; Good, M.R. Unitary evaporation via modified Regge-Wheeler coordinate. In Proceedings of the 15th Marcel Grossmann Meeting on Recent Developments in Theoretical and Experimental General Relativity, Astrophysics, and Relativistic Field Theories, Rome, Italy, 1–7 July 2018.
43. Good, M.R.R.; Ong, Y.C. Signatures of Energy Flux in Particle Production: A Black Hole Birth Cry and Death Gasp. *J. High Energy Phys.* **2015**, *1507*, 145. [CrossRef]
44. Good, M.R.R. Reflecting at the Speed of Light. In *Memorial Volume for Kerson Huang*; World Scientific: Singapore, 2017; pp. 113–116. [CrossRef]
45. Chen, P.; Ong, Y.C.; Yeom, D.H. Black Hole Remnants and the Information Loss Paradox. *Phys. Rep.* **2015**, *603*, 1–45. [CrossRef]
46. Ford, L. Quantum Coherence Effects and the Second Law of Thermodynamics. *Proc. R. Soc. Lond. A* **1978**, *A364*, 227–236. [CrossRef]
47. Davies, P. Can Moving Mirrors Violate the Second Law of Thermodynamics? *Phys. Lett. B* **1982**, *113*, 215–218. [CrossRef]
48. Walker, W. Negative Energy Fluxes and Moving Mirrors in Curved Space. *Class. Quantum Gravity* **1985**, *2*, L37. [CrossRef]
49. Ford, L. Constraints on negative energy fluxes. *Phys. Rev. D* **1991**, *43*, 3972–3978. [CrossRef]
50. Ford, L.; Roman, T.A. The Quantum interest conjecture. *Phys. Rev. D* **1999**, *60*, 104018. [CrossRef]
51. Ford, L.; Roman, T.A. Energy flux correlations and moving mirrors. *Phys. Rev. D* **2004**, *70*, 125008.. [CrossRef]
52. Good, M.R.R.; Linder, E.V. Slicing the Vacuum: New Accelerating Mirror Solutions of the Dynamical Casimir Effect. *Phys. Rev. D* **2017**, *96*, 125010. [CrossRef]
53. Cong, W.; Qian, C.; Good, M.R.; Mann, R.B. Effects of Horizons on Entanglement Harvesting. *arXiv* **2020**, arXiv:gr-qc/2006.01720.
54. Bianchi, E.; Smerlak, M. Entanglement entropy and negative energy in two dimensions. *Phys. Rev. D* **2014**, *90*, 041904. [CrossRef]
55. Good, M.R.; Linder, E.V.; Wilczek, F. Moving mirror model for quasithermal radiation fields. *Phys. Rev. D* **2020**, *101*, 025012. [CrossRef]
56. Su, D.; Ho, C.M.; Mann, R.B.; Ralph, T.C. Black Hole Squeezers. *Phys. Rev. D* **2017**, *96*, 065017. [CrossRef]